

Comprehensive Modeling of Large Photovoltaic Systems for Heterogeneous Parallel Transient Simulation of Integrated AC/DC Grid

Ning Lin ¹, Member, IEEE, Shiqi Cao ¹, Student Member, IEEE, and Venkata Dinavahi ¹, Fellow, IEEE

Abstract—Detailed nonlinear transient modeling of the photovoltaic (PV) system enables an accurate study of the host integrated AC/DC grid. In this article, the parallel architecture of the graphics processing unit (GPU) catering to a massive number of PV modules is utilized in conjunction with CPU for efficient transient simulation. To reflect the exact operation status of the solar power system subjected to various temperatures and nonuniform solar irradiance in the electromagnetic transient (EMT) simulation, all necessary panels are modeled individually, and therefore, a scalable PV array model with a flexible level of aggregation is proposed in addition to its fully detailed discrete counterpart so as to improve the computational efficiency. The single-instruction multiple-thread implementation mode of the GPU enables up to 10 million PV panels, regardless of the size or type, to be computed concurrently, and noticing that the hybrid AC/DC grid has a significant irregularity, the CPU is also adopted to tackle systems with inadequate parallelism. Meanwhile, since the AC grid dynamic interaction has a distinct tolerance on the time-step to that of the remaining part, a multi-rate scheme is employed to expedite the heterogeneous CPU-GPU computation for dynamic-EMT co-simulation, whose results are validated by the commercial off-line tools MATLAB/Simulink and DSATools/TSAT.

Index Terms—AC/DC grid, dynamic simulation, electromagnetic transients, graphics processing unit (GPU), multi-terminal DC, parallel processing, photovoltaic, transient stability.

I. INTRODUCTION

THE RENEWABLE energy generated by the photovoltaic (PV) effect has witnessed a dramatic increase in its proportion in power generation worldwide [1]. The high-voltage direct current (HVDC) transmission is an effective interface to link solar power plants with a capacity of dozens or even hundreds of megawatts in remote areas to the major grid [2]. While being environment-friendly, the vulnerability of large-scale PV installations to the weather condition is potentially hazardous to

the safe operation of the overall power system [3]–[5]. Therefore, a number of commercial transient simulation tools were developed and used extensively to study their impact on AC and DC grids that form an integrated AC/DC grid [6].

A heavy burden exists in computing a comprehensive AC/DC grid, especially the detailed PV systems due to its nonlinear transcendental i - v relationship, and therefore efforts have been made to shorten the simulation time [7]–[10]. Reasonable model simplification is conducted to improve the simulation efficiency, e.g., the average value model of the modular multi-level converter (MMC) justifies itself in the AC grid stability analysis when power flow is a major concern [11]. Nevertheless, it should be noted that the omission of modeling details even disqualifies the MMC detailed equivalent model from accurate electromagnetic transient (EMT) simulation. Similarly, lumping together all the solar panels hinders a thorough investigation of the hybrid grid; however, a tremendous computational burden on the predominant CPU restricts the scale of the detailed PV array model [12] and the renewable energy source was always greatly simplified [13], [14]. Thus, detailed modeling of a massive number of PV modules has remained a major obstacle to efficient EMT simulation.

In the power system with a high penetration of renewable energy, a number of factors, especially the weather, have influence on the power flow which in turn affects the operation and stability of the synchronous generators in the AC grid [15], [16]. Since a PV plant normally covers a wide region, the irradiation every panel receives could vary significantly, and it is quite common to encounter partial shading [17]–[19]. Theoretically, the total output power of a PV station can be calculated precisely if each PV panel is taken individually. However, computing hundreds of thousands or even millions of PV models using the Newton-Raphson iteration method pose a remarkable challenge to the capacity of CPU [20], which accounts for the prevalence of the lumped model albeit it is unable to reflect their uniqueness.

High-performance computing using the graphics processing unit (GPU) has been gaining momentum in the EMT simulation of large-scale power systems and power converters that exhibit a high regularity [21]–[23]. It provides a solution to retaining a high fidelity of the PV systems in EMT simulation. Though it outweighs CPU in parallelism, the GPU has a much lower frequency, e.g., the Nvidia Tesla V100 has a boosted clock of 1530 MHz [24], which indicates that processing the AC/DC grid is more challenging than the previously studied systems

Manuscript received August 1, 2019; revised November 23, 2019 and December 31, 2019; accepted January 12, 2020. Date of publication January 15, 2020; date of current version May 20, 2020. This work was supported in part by the Natural Science and Engineering Research Council of Canada. Paper no. TEC-00804-2019. (Corresponding author: Ning Lin.)

The authors are with the Department of Electrical and Computer Engineering, University of Alberta, Edmonton, Alberta T6G 2V4, Canada (e-mail: ning3@ualberta.ca; sc5@ualberta.ca; dinavahi@ualberta.ca).

Color versions of one or more of the figures in this article are available online at <https://ieeexplore.ieee.org>.

Digital Object Identifier 10.1109/TEC.2020.2966729

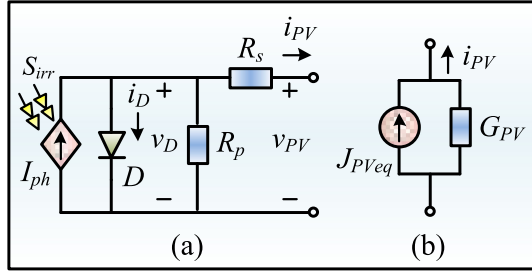


Fig. 1. PV unit model: (a) Equivalent circuit, and (b) EMT model.

due to a large portion of inhomogeneities, i.e., there are more components whose number is insufficient to support massive parallelism, and consequently the GPU performance is adversely affected.

Therefore, the EMT-dynamic co-simulation using a heterogeneous CPU-GPU platform is proposed in this work for studying the AC/DC grid. Any components with a sufficient quantity are computed on the GPU to fully exploit its single-instruction multiple-thread (SIMT) implementation feature, especially the PV panels for which a scalable model is proposed to cater to the high fidelity requirement. The CPU, on the other hand, is in charge of those less repetitive, e.g., the IEEE 39-bus system as AC grid. The multi-rate scheme is investigated to further improve the simulation efficiency considering that the EMT and dynamic simulations have distinct time-steps.

This paper is organized as follows: Section II proposes the detailed scalable PV array model. In Section III, the integrated AC/DC grid is specified, followed by Section IV where the heterogeneous computational architecture of the hybrid grid on mixed CPU-GPU is presented. The co-simulation results are provided and analyzed in Section V, and the conclusions are drawn in Section VI.

II. DETAILED PHOTOVOLTAIC SYSTEM EMT MODEL

A. Basic PV Unit

Fig. 1(a) shows the single-diode equivalent circuit of a basic PV unit whose photoelectric effect is represented by the irradiance-dependent current source [25]

$$I_{ph} = \frac{S_{irr}}{S_{irr}^*} \cdot I_{ph}^* (1 + \alpha_T \cdot (T_K - T_K^*)), \quad (1)$$

which has variables with the superscription * as references, S_{irr} as the solar irradiance, α_T the temperature coefficient, and T_K the absolute temperature. In addition, the model is also comprised of the shunt and series resistors R_p and R_s , respectively, and the anti-parallel diode D which has the following exponential i - v characteristics

$$i_D(t) = I_s \cdot \left(e^{\frac{v_D(t)}{V_T}} - 1 \right), \quad (2)$$

where I_s is the saturation current, and V_T denotes the thermal voltage. After discretization using partial derivatives for EMT computation, the nonlinear diode yields an equivalent

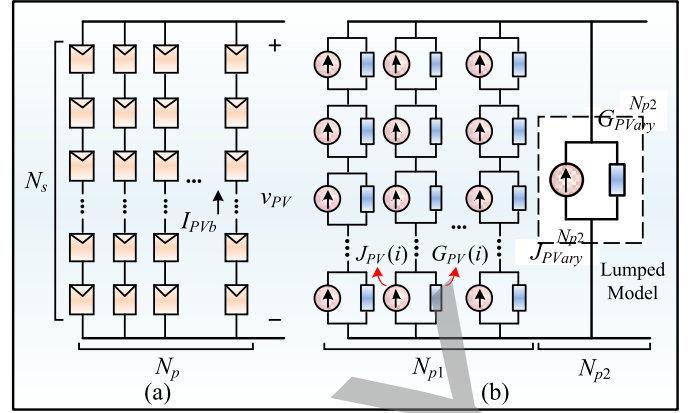


Fig. 2. An arbitrary array of PV panels: (a) PV array of $N_p \times N_s$ panels, and (b) the scalable EMT model.

conductance G_D and current I_{Deq} , as expressed by

$$G_D = \frac{\partial v_D(t)}{\partial i_D(t)} = \frac{I_s}{V_T} \cdot e^{\frac{v_D(t)}{V_T}}, \quad (3)$$

$$I_{Deq} = i_D(t) - G_D \cdot v_D(t). \quad (4)$$

Therefore, with all of its components represented by current sources and conductors or resistors, the PV unit can be converted into the most concise two-node Norton equivalent circuit, as shown in Fig. 1(b), where

$$J_{PVeq} = \frac{I_{ph} - I_{Deq}}{G_D R_s + R_s R_p^{-1} + 1}, \quad (5)$$

$$G_{PV} = \frac{G_D + R_p^{-1}}{G_D R_s + R_s R_p^{-1} + 1}. \quad (6)$$

B. Scalable PV Array Model

In large-scale PV plants, a substantial number of panels are arranged in an array in the centralized configuration in order to generate sufficient energy to an inverter that the whole array connects to. For an arbitrary PV array with N_p parallel strings each of which containing N_s series panels, as shown in Fig. 2(a), the equivalent circuit in Fig. 1(a) is still applicable in describing its i - v characteristics, expressed by

$$i_{PV}(t) = N_p I_{ph} - N_p I_s \cdot \left(e^{\frac{v_{PV}(t) + N_s N_p^{-1} R_s i_{PV}(t)}{N_s V_T}} - 1 \right) - G_p (i_{PV}(t) R_s + N_p N_s^{-1} v_{PV}(t)), \quad (7)$$

when the lumped model is adopted. The transcendental equation cannot be discretized directly in an identical manner as of (3) and (4). Therefore, using the same method, each component in the Thévenin or Norton equivalent circuit of the lumped PV model is calculated separately and then aggregated, leading to the equivalent conductance and current G_{PVary} and J_{PVary} with a similar form to (5) and (6).

A major shortcoming of the lumped model is that the characteristics of PV panels subjected to the various environment – most notably the solar irradiance – cannot be revealed in this

case, for example, when the irradiance exhibits the normal distribution, as

$$f(S_{irr}|\mu, \sigma^2) = \frac{1}{\sqrt{2\pi}\sigma} e^{-\frac{(S_{irr}-\mu)^2}{2\sigma^2}}, \quad (8)$$

where μ is the mean value of the distribution, and σ denotes the standard deviation. Therefore, the performance of each PV panel needs to be considered to achieve the highest simulation fidelity, meaning a $N_p \times N_s$ array corresponds to an admittance matrix virtually 4 times larger in its dimension undergoing the Newton-Raphson iteration that makes the simulation extremely slow. The Norton equivalent circuit lays the foundation for a simple solution, as based on (5) and (6), by first merging all N_s panels in every string and then the N_p branches, the equivalent circuit of an array can be derived as

$$G_{PV\ array} = \sum_{i=1}^{N_p} \left(\sum_{j=1}^{N_s} G_{PV}^{-1}(i, j) \right)^{-1}, \quad (9)$$

$$J_{PV\ array} = \sum_{i=1}^{N_p} \left[\sum_{j=1}^{N_s} (J_{PV}(i) G_{PV}^{-1}(i)) \cdot \left(\sum_{j=1}^{N_s} G_{PV}^{-1}(i) \right)^{-1} \right]. \quad (10)$$

where i denotes an arbitrary PV board along with j .

Nevertheless, aggregating millions of PV panels in one or a number of plants still constitutes a tremendous computational burden on the CPU, because (3)–(10) other than (7) need to be calculated repeatedly at every time instant. Noticing that it is not necessary to distinguish every panel from each other, as a large proportion of the panels normally operate under virtually the same condition, a scalable PV array model is proposed to utilize the low computational burden achieved by the lumped model while in the meantime retaining a maximum possible individuality of the remaining panels.

In Fig. 2(b), a flexible number of $N_{p1} \times N_s$ panels in the $N_p \times N_s$ array are modeled in detail, and consequently the lumped model is applied to the rest $N_{p2} = N_p - N_{p1}$ strings. As an outcome of the hybrid modeling method, the overall EMT model of a PV array can be derived by summation

$$G_{PV\ array} = G_{PV\ array}^{N_{p2}} + \sum_1^{N_{p1}} \left(\sum_1^{N_s} G_{PV}^{-1}(i) \right)^{-1} \quad (11)$$

$$J_{PV\ array} = J_{PV\ array}^{N_{p2}} + \sum_1^{N_{p1}} \left[\sum_1^{N_s} [J_{PV}(i) G_{PV}^{-1}(i)] \cdot \left[\sum_1^{N_s} G_{PV}^{-1}(i) \right]^{-1} \right]. \quad (12)$$

The selection of N_{p1} is determined primarily by the simulation accuracy since it is obvious that a zero N_{p1} means the scalable model degenerates into the absolute lumped model, while more PV panels are depicted when N_{p1} approaches N_p . Therefore, N_{p1} is defined as a variable in the program to leave sufficient room for adjustment so that a tradeoff between simulation

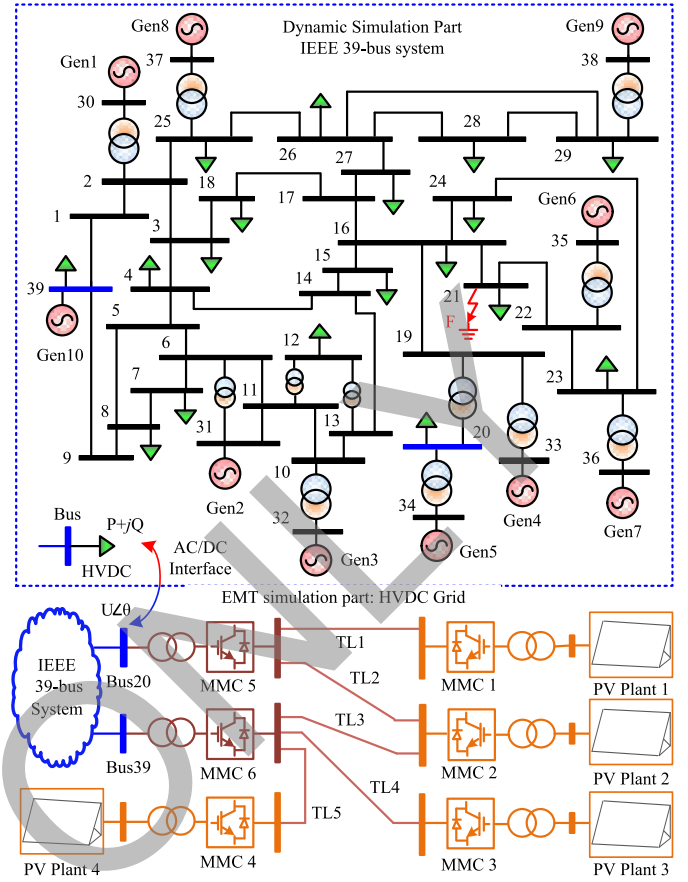


Fig. 3. IEEE 39-bus system integrated with DC grid connected to PV plants.

efficiency and the extent of information to be revealed can be made. The combination of lumped and discrete PV parts enables less computational work on the processors; in the meantime, since both models share virtually identical equations, it is not necessary to distinguish them when parallel processing is carried out.

III. INTEGRATED AC/DC GRID

Fig. 3 shows the integrated AC/DC grid comprising of the following three parts: the AC grid based on the IEEE 39-bus system, the multi-terminal DC grid where stations MMC_5 and MMC_6 are inverters while the other 4 are rectifiers, and the 4 PV farms with each having a capacity of 500 MW. The transient stability is of concern in the IEEE 39-bus system and therefore dynamic simulation is conducted; on the contrary, EMT simulation is required to reveal the exact behavior of the PV farms as well as the DC grid.

A. AC Grid

The transient stability analysis of the AC grid is conducted based on the following set of differential-algebraic equations:

$$\dot{\mathbf{x}} = \mathbf{f}(\mathbf{x}, \mathbf{u}, t), \quad (13)$$

$$\mathbf{g}(\mathbf{x}, \mathbf{u}, t) = 0, \quad (14)$$

where \mathbf{x} and \mathbf{u} denote the state variable vector and the bus voltages, respectively. To enable the dynamic simulation starts properly, the initial conditions should be set, e.g.,

$$\mathbf{x}_0 = \mathbf{x}(t_0). \quad (15)$$

The differential equation describes the dynamics of the synchronous generators using the 9th-order model. It should be discretized prior to the solution, as it takes the form of

$$\mathbf{x}(t) = \mathbf{x}(t - \Delta t) + \frac{\Delta t}{2} (\mathbf{f}(\mathbf{x}, \mathbf{u}, t) + \mathbf{f}(\mathbf{x}, \mathbf{u}, t - \Delta t)), \quad (16)$$

when the 2nd-order Trapezoidal rule is applied, where the vector \mathbf{x} contains the 9 generator states

$$\mathbf{x} = [\delta, \Delta\omega, \psi_{fd}, \psi_{1d}, \psi_{1q}, \psi_{2q}, v_1, v_2, v_3]. \quad (17)$$

The first two variables, the rotor angle and angular speed derivative, are used in the motion equation, the flux ψ is used to describe the rotor electrical circuit, and the voltages $v_{1,2,3}$ appear in the excitation system.

Following the solution of the differential equation, the algebraic equation representing the network can also be solved in conjunction with the generator's stator equations

$$\begin{bmatrix} \mathbf{I}_m \\ \mathbf{I}_r \end{bmatrix} = \begin{bmatrix} \mathbf{Y}_{mm} & \mathbf{Y}_{mr} \\ \mathbf{Y}_{rm} & \mathbf{Y}_{rr} \end{bmatrix} \begin{bmatrix} \mathbf{V}_m \\ \mathbf{V}_r \end{bmatrix}, \quad (18)$$

where m is the number of synchronous generator nodes, and r is the number of remaining nodes in the network.

B. Multi-Terminal DC System

The DC system terminals employ the modular multi-level converter which has two prevalent models, i.e., the averaged-value model and the detailed equivalent model. The former type is preferred in power flow analysis for its simplicity, while the latter one provides full details, especially in case of DC faults when the diode freewheeling effect cannot be revealed by its counterpart.

It is time-consuming to simulate the MMC in its full detail due to the repetitive computation of a remarkable number of submodules (SMs) included for safe operation as well as a large admittance matrix it presents. When a half-bridge submodule is under normal operation, its terminal voltage can be found as a function of upper switch gate signal V_g :

$$v_{SM,k}(t) = i_{SM,k}(t) \cdot r_{on} + V_{g,k}(t) \int_{t_1}^{t_2} \frac{i_{SM,k}(t)}{C_{SM,k}} dt, \quad (19)$$

where k represents an arbitrary submodule, r_{on} is the on-state resistance of a power semiconductor switch, $C_{SM,k}$ is the DC capacitor voltage, and $i_{SM,k}$ equals to the arm current i_{arm} where it locates. A methodology for avoiding large admittance matrix is therefore available since all the submodules can be taken as a voltage source with a value of $v_{SM,k}$, which can be summed conveniently; in the meantime, investigation of the submodule operation status becomes independent from overall MMC circuit solution. Specifically, in EMT simulation, a detailed MMC arm

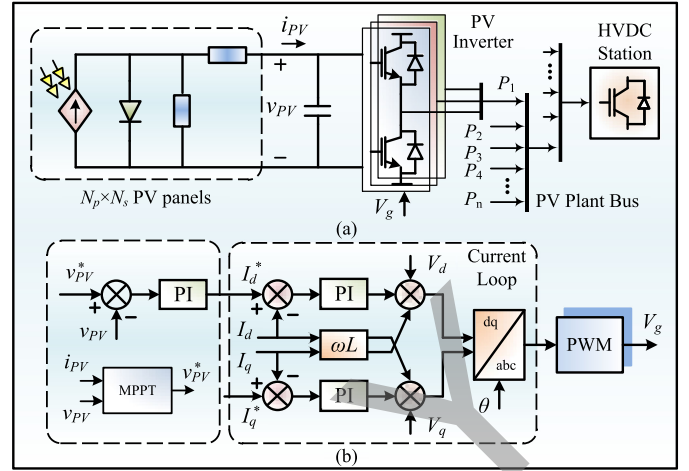


Fig. 4. Schematic of HVDC rectifier station AC side: (a) Aggregation of PV inverters, and (b) PV inverter controller.

takes the form of

$$v_{arm}(t) = \sum_{k=1}^N v_{SM,k}(t) + i_{arm}(t) \cdot Z_{Lu,d} + 2v_{Lu,d}^i(t), \quad (20)$$

where $Z_{Lu,d}$ is the impedance of the arm inductor $L_{u,d}$, $v_{Lu,d}^i$ is the incident pulse in transmission line modeling of an inductor [26]. It can be noticed that all submodules are excluded from the arm to attained a low-dimension admittance matrix which consequently contributes to the improvement on computational efficiency.

C. PV Plant

As shown in Fig. 4(a), a large-scale PV plant normally has a capacity of dozens to hundreds of megawatts sustained by a considerable number of inverters. An inverter with a rated power of 1MW is able to accommodate an array of up to 200×25 1STH-215-P PV panels manufactured by 1 SolTech INC. Therefore, a group of PV plants with a total rating of thousands of megawatts is literally comprised of thousands of PV inverters which reach the criterion of massive parallelism.

Fig. 4(b) shows that each PV inverter regulates its own DC voltage exerted on the PV array using maximum power point tracking, which is in charge of calculating an optimized voltage that enables the maximum output power, and consequently it is deemed as the voltage reference in the controller based on d - q frame. Then, the inverter DC side voltage is found as

$$V_{PV,DC} = (G_C + G_{PVary})^{-1} (I_{PV,DC} + J_{PVary} + 2v_C^i(t)), \quad (21)$$

where G_C and v_C^i are the conductance and incident pulse of a capacitor modeled by a lossless transmission line, $V_{PV,DC}$ and $I_{PV,DC}$ are PV inverter DC side voltage and current, respectively. Then, all PV inverter powers are summed and taken as the input of a rectifier station in the DC grid.

Following the solution of PV inverter DC side, the internal node of the diode in the PV module should be updated, where

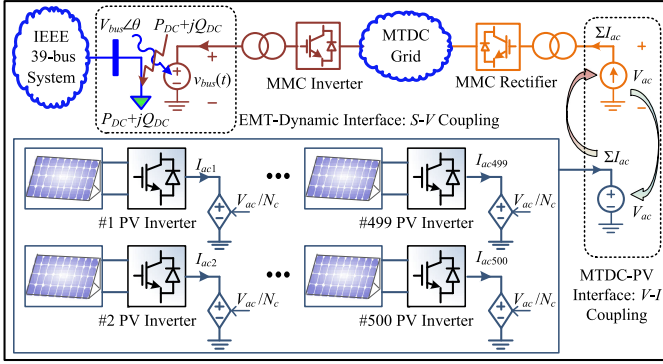


Fig. 5. Interfaces for integrated AC/DC grid EMT-dynamic co-simulation.

its voltage v_D at the simulation instant t takes the form of

$$v_D(t) = -I_{PV,b} \cdot (G_D + R_p^{-1})^{-1} + V_{PV,b}, \quad (22)$$

with the branch voltage and current expressed as

$$V_{PV,b} = \frac{(I_{ph} - I_{Deq})}{G_D + R_p^{-1}}, \quad (23)$$

$$I_{PV,b} = J_{PV,b} - V_{PV,DC} \cdot G_{PV,b}. \quad (24)$$

It should be noted that the branch variables with subscription b could be either the lumped or the discrete part in the proposed scalable PV array model.

D. EMT-Dynamic Co-Simulation Interfaces

It would be impractical to take the AC system undergoing transient stability analysis and its EMT-simulation DC counterpart as one computing objective since the two types are not instantly compatible. Thus, a power-voltage-based interface is introduced to enable the availability of two transient simulations of one integral system. As illustrated in Fig. 5, since the power flow is the principal variable in dynamic simulation, the external DC grid can be taken as a load to the AC bus it connects to and converted into the conductance by

$$Y_{DC} = \frac{(P_{DC} + j \cdot Q_{DC})}{V_{Bus}^2}, \quad (25)$$

where P_{DC} and Q_{DC} are the MMC-based inverter AC side active and reactive powers obtained in EMT simulation, respectively, and V_{bus} denotes the bus voltage amplitude. Consequently, by taking the DC grid as conductance Y_{DC} , the AC grid constitutes an independent subsystem that undergoes solely the transient stability analysis.

On the other hand, solution of the algebraic equation in the dynamic simulation yields the AC bus voltage V_{bus} in conjunction with its phase angle θ as a complex variable under $d-q$ frame, which is, in fact, the input of the inverter station in EMT simulation. As a result, the two types of simulations conducting separately become interactive and the co-simulation is realized by exchanging the complex power-voltage signals on both sides of the AC/DC grid.

Although both the MTDC grid and the PV plant run the same type of simulation, linking the MMC with hundreds of PV inverters leads to a huge electrical system. A pair of coupled voltage-current sources is inserted between them to avoid a heavy computational burden. Since the MMC controls the instantaneous AC side voltage V_{ac} , the PV inverters are connected to the voltage source V_{ac}/N_c where N_c is a coefficient reflecting the winding turn ratio of the transformer between the PV inverter and the MMC converter transformer. Then, each PV inverter constitutes an independent circuit that can be solved without the participation of its counterparts as well as the MTDC grid. The instantaneous current obtained from the solution can then be added together and sent to the MMC AC side current source to enable the DC grid solution, which in turn prepares the AC voltage for the next time-step.

IV. HETEROGENEOUS CPU-GPU COMPUTING

A. CPU-GPU Program Architecture

Extensive parallelism exists in both the AC and DC grid, especially the 4 PV plants. For example, the AC grid has 10 synchronous generators and 39 buses; the DC grid, depending on the model, may contain thousands of submodules, and it connects to millions of PV panels.

While the handling of PV plants accounts for the major computational burden of simulating the integrated power system, the remaining equipment also has a significant contribution. The number of a circuit component type determines where and subsequently how it will be processed. The 4 PV stations and the detailed MMC model show a high homogeneity and therefore both of them are allocated to the GPU for parallel processing under the SIMT mode which ensures a particularly efficient implementation. On the contrary, the number of buses or synchronous generators in the AC grid falls short of massive parallelism, and so is the DC grid if the AVM is adopted, making CPU the better option.

Therefore, heterogeneous computing of the hybrid AC/DC grid is based on the CPU-GPU architecture termed as host and device. On the device, taking apart the two the types of PV models in the scalable array will jeopardize the parallelism as both may have a large quantity. The capability of the SIMT mode being tolerant to slight differences between the lumped model and the discrete PV model enables their computation by one GPU global function, or terminologically, the same kernel using the programming language CUDA C [27].

Determined by the number of threads, various kernels are designed to describe the PV system and the MMC. For example, in Fig. 6, processing all PV panels is divided into 6 stages. The first kernel initializes the model parameters, followed by the second kernel which deals with model discretization. Since both processes are applicable to every PV panel, either in lumped or discrete form, both kernels need to launch a total number of $N_{PV} \times (N_{p1} \cdot N_s + 1)$ threads, where N_{PV} denotes the total number of PV inverters. The third kernel is specifically designed for the discrete PV panels which need to be aggregated and therefore the total thread number is $N_{PV} \times N_{p1}$. Dealing with calculations of all PV inverters in the following two kernels

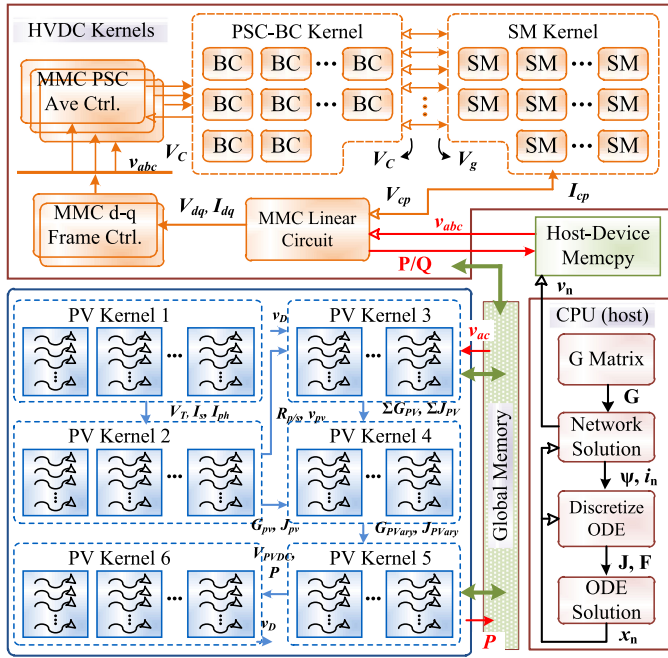


Fig. 6. CPU-GPU co-simulation program architecture.

means that the thread number shrinks to N_{PV} temporarily before it recovers in the last kernel which updates the circuit information for the next time-step. As can be seen, data exchange between various kernels occurs frequently, and therefore, all those variables are stored in the global memory to enable convenient access.

Though the above process demonstrates that numerous threads are invoked by the same kernel, the content of each thread, including the PV parameters, could be different, and this individuality is achieved by proper identification of the thread. Consequently, the compatibility of various PV module types and their parameters extends the parallelism to the maximum possible level. In this context, the selection of either one or a few PV module types does not affect the computing speed since the mere difference between these two options is the parameter initialization, which occurs only once and the burden it imposes on the processors is negligible compared with that of the bulk program of integrated AC/DC grid. Nevertheless, to reflect the geographical and atmospheric impacts on the PV farms and the power system, different PV parameters, including irradiance and temperature, are considered at the initial stage of the co-simulation.

Similarly, the detailed MMC model is computed in 5 steps. The MMC main circuit connecting to the AC grid receives the bus voltage from the dynamic simulation on CPU and following its solution, the AC side current can be derived and sent to the controller based on the $d-q$ frame. Phase-shift control (PSC) strategy is adopted for the MMC internal submodule voltage regulation [28]. The Averaging (Ave) Control as its first part seeks the desired mean of DC capacitor voltages in a phase, whilst the second part, the Balancing Control (BC) in charge of balancing all submodule voltages has a corresponding quantity and therefore the kernel invokes a massive number of threads.

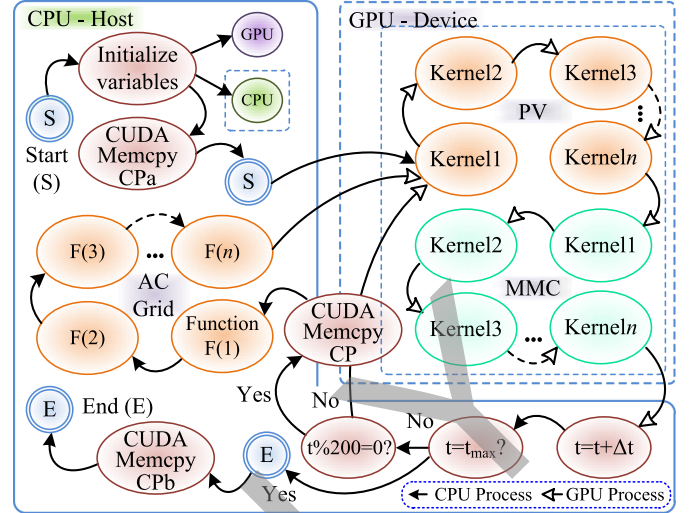


Fig. 7. Heterogeneous CPU-GPU computation implementation.

The AC grid divided into 4 major parts, on the other hand, is in a strictly sequential manner on a single CPU processor. The solution of the network equations along with the differential equation yields all bus voltages, among which those connected to the HVDC stations are sent to the GPU using CUDA memory copy. Similarly, the power is returned to the host for calculating the admittance matrix of the AC network.

B. Co-Simulation Implementation

Sharing of the computational burden by CPU in dealing with part of the system distinguishes the proposed heterogeneous computing from pure CPU or GPU execution. Nevertheless, the initialization process still needs to take place in the host, when all variables on both processors are defined. Once the co-simulation starts, all CPU functions and GPU kernels are implemented in a largely sequential manner, e.g., the kernels of PV plants are invoked one after another first, followed by those of the MMC, and later the CPU functions on the host to complete an intact cycle before returning to the PV kernels on the GPU again, as given in Fig. 7.

The two processors, as can be noticed, are not interactive unless the information is exchanged using the CUDA C command `cudaMemcpy`. However, the two programs have a common timeline since the co-simulation is generally on the host-device framework and the GPU kernels are able to access to the time instant defined on the CPU as an incremental value without memory copy. Meanwhile, the fact that the AC grid dynamic simulation is able to tolerate a much larger time-step than the EMT simulation enables the adoption of multi-rate implementation, i.e., the program on CPU runs at a time-step of 10 ms, 200 times larger than that of EMT simulation. Therefore, data exchange between the two processors only takes place when the CPU program starts to implement.

After the simulation reaches the end, those concerned variables are gathered for system analysis.

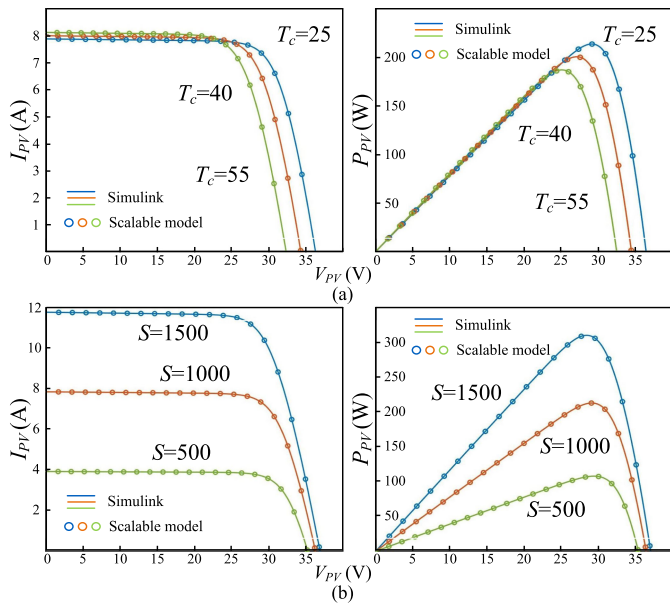


Fig. 8. Basic PV module i - v and P - v characteristics with: (a) Different cell temperatures and $S = 1000 \text{ W/m}^2$, and (b) various irradiances and $T_c = 25^\circ \text{C}$.

It can be seen that a universal heterogeneous computing approach is proposed for the AC/DC grid EMT-dynamic co-simulation. The processing algorithm, along with the program architecture, is not reliant on any specific type of GPU, let alone CPU since all the functions involved in the design are fundamental to a variety of CPU-GPU platforms.

V. EMT-DYNAMIC CO-SIMULATION RESULTS

The CPU-GPU co-simulation of the AC/DC grid involving detailed massive PV panels is conducted on a 64-bit operating system with 80 Intel Xeon CPU E5-2698 v4 processors, 192 GB memory, and the NVIDIA Tesla V100 GPU. A few commercial simulation tools, including MATLAB/Simulink and DSAtools for EMT and dynamic simulation respectively are resorted. An experimentally verified PV model in the former tool [12], [29] is adopted for comparison with the proposed model; whilst the latter tool has been extensively used and heavily relied on for power system planning and design. Therefore, an indirect but reliable validation is carried out considering that it is impractical to experimentally test the entire integrated AC/DC grid.

A. PV Array

The accuracy of proposed scalable PV model is tested using two configurations, i.e., 1×1 and 2×25 considering that the computational capability of the off-line EMT-type solver will be soon overwhelmed if the array keeps expanding. Fig. 8(a) shows that when a single PV module is under a constant irradiance, a lower temperature leads to a larger current at the maximum power point and consequently the power; the intuitive i - v relationships under different irradiances are quantified in Fig. 8(b), which also demonstrates that the proposed model has an exact performance to that of the Simulink model.

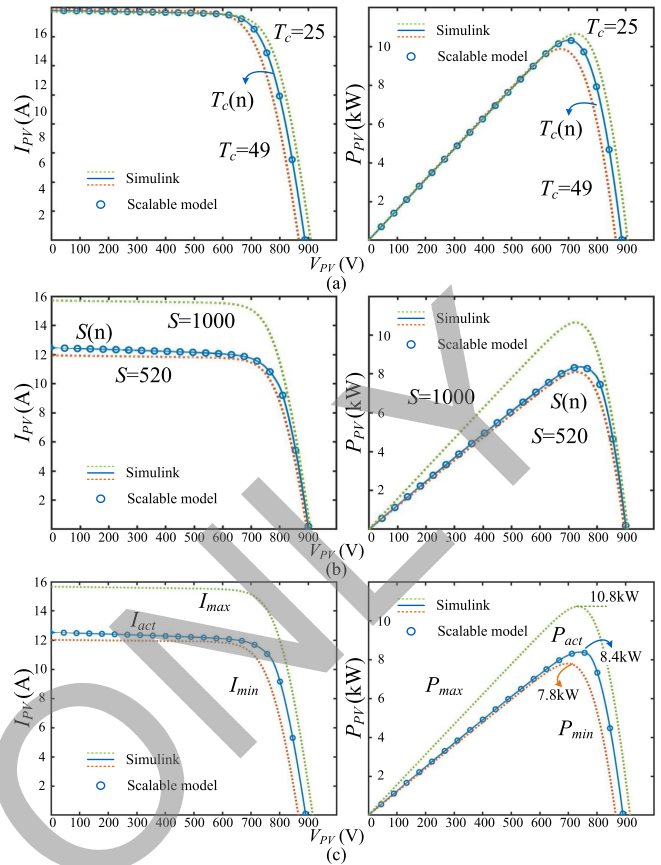


Fig. 9. Performance of 2 PV branches under various: (a) Cell temperatures and $S = 1000 \text{ W/m}^2$, (b) irradiances and $T_c = 25^\circ \text{C}$, and (c) temperatures and irradiances.

In the 2×25 array, one string of 25 series boards is represented by the lumped PV model with a constant irradiance of 1000 W/m^2 and a temperature of 25°C , while the other string is formed by cascaded discrete modules to reveal the impact of the environmental conditions. Fig. 9(a) shows the i - v characteristics of the array when the discrete 25 panels have a temperature distribution from 25°C to 49°C with a linear incremental of 1°C . It indicates that the output current, and consequently the power, of the overall 2-string array neither equals to the upper or lower limits when all boards have a unified temperature of 25 or 49°C . In Fig. 9(b), the 25 discrete PV panels are subjected to 520 to 1000 W/m^2 irradiances with an incremental of 20 W/m^2 per board. It shows that the actual output power is close to the lower limit when all those in the second branch receives 520 W/m^2 ; nevertheless, the latter could by no means represent the former when both irradiances and temperature vary, as proven in Fig. 9(c) which exhibits a minimum gap of 0.6 kW , and the difference will be amplified significantly once hundreds of thousands of branches are taken into consideration.

The scalable PV model performance under extreme conditions was also tested for accuracy validation. In Fig. 10(a), the same 2×25 PV array is subjected to 2 low ambient temperatures, i.e., -10°C and -20°C . The maximum output power remains below 300 W when the irradiance is 20 W/m^2 . A dramatic increase of two orders of magnitude was witnessed when one

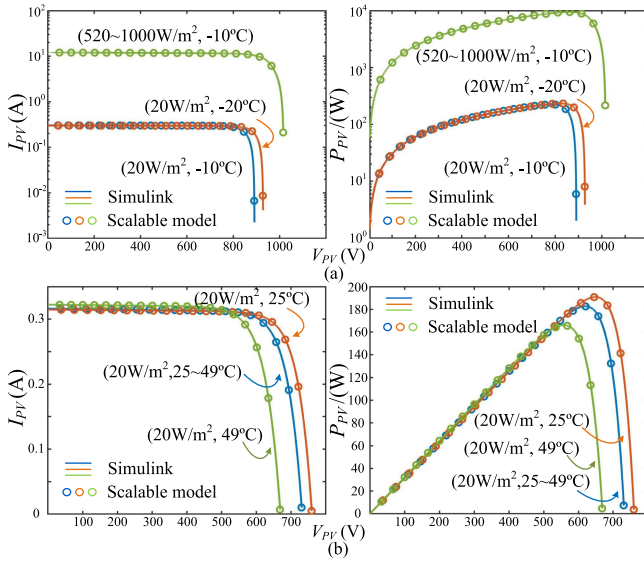


Fig. 10. Performance of 2 PV branches under extreme conditions: (a) Low temperature operation, and (b) low irradiance operation.

TABLE I
SIMULATION SPEED COMPARISON BETWEEN GPU AND CPU

$N_{p1}:N_{p2}$	Module No.	GPU	CPU	MC-CPU	Sp1	Sp2
1:199	4.48×10^5	18.7s	224s	34.7s	12	1.9
10:190	8.8×10^5	47.3s	2320s	373s	49	7.9
50:150	2.8×10^6	223s	11502s	2231s	52	10
100:100	5.2×10^6	482s	22642s	4226s	47	8.8
150:50	7.6×10^6	946s	31486s	10386s	33	11
199:1	9.952×10^6	1139s	39292s	13800s	34	12

of the branches receives solar irradiance ranging from 520 to 1000 W/m^2 . Fig. 10(b) shows that the proposed model still has the same behavior as the off-line simulation tool under low irradiance and normal temperature, and once again the low output powers prove that temperature variation has a less significant impact on the total output of a PV array than the irradiance. The exact match to the off-line simulation tool's outcomes in all above tests indicate that the proposed scalable PV model has an identical performance to a real module, meaning it can be used for simulating a much larger system whilst commercial offline simulation tools fall short of doing so due to an extraordinary computational burden.

The performance of the aforementioned processors in carrying out a 10 s simulation of 2000 MW PV plants with a massive number of panels is summarized in Table I. Even when the ratio of discrete and lumped PV branches is 1:199, i.e., there are 448,000 equivalent circuits, the GPU is still able to gain a speedup of 12 (Sp1) and 1.9 (Sp2) respectively over the default single CPU and multi-core CPU, let alone when the number of equivalent circuits reaches approximately 10 million when the ratio is 199. With a medium level of detail, the GPU is able to achieve a speedup over the prevalent CPU simulation of around 50 times. Even when the multi-core CPU approach yet to be exploited for circuit computing is adopted using OpenMP, the Tesla V100 GPU is still about 10 times more efficient. A decent

speedup of up to 5 times is maintained over the 80-core CPU even if a common platform with 12 Intel Xeon CPU E5-2620 processors, 16 GB memory, and the NVIDIA GTX 1080 GPU takes over the co-simulation, when the computing duration for the 6 combinations of N_{p1} and N_{p2} are 31.2 s, 152.3 s, 686.8 s, 1348 s, 2035 s, and 2675 s, respectively. It should be noted that although the GPU is always more efficient than CPU as well as its multi-core configuration regardless of the proportion that those discrete PV panels account for, the smallest possible N_{p1} should always be selected to avoid unnecessary numerical operations, especially when a large number of PV panels have virtually identical operation conditions, including irradiance and temperature.

B. AC/DC Grid Interaction

The penetration of PV energy into the power system means that the AC grid transient stability is highly vulnerable to the momentary change of weather. If the solar irradiance of all 10 million PV panels in 4 stations conforms to normal distribution, with a mean value $\mu = 1000 W/m^2$ and $\sigma = 100$, the actual output power of a station is approximately 430 MW, which has a vast difference to over 530 MW under a uniform average irradiance, meaning the proposed scalable model enables the derivation of exact output power of a PV station and consequently, its impact on the AC/DC grid can be correctly studied. In contrast, the transient stability analysis results will be erroneous and misleading for power system planning and operation if the lumped model is adopted, as the 100 MW disparity will be further amplified following the integration of more PV stations into the grid.

When the mean μ reduces from 1000 W/m^2 to 700 W/m^2 and 500 W/m^2 between 20 s and 25 s at Plant 3 and 4, their output power climbs down to 270 MW and 160 MW, respectively. As a result, the inverter station MMC_5 witnesses a roughly 430 MW reduction while the power at MMC_6 only sees a momentarily fluctuation before it restores μ in 10 secs, as given in Fig. 11(a). It turns out in Fig. 11(b) that the AC grid is unstable with the frequency decreasing below the minimum 59.5 Hz. Therefore, 255 MW and 195 MW of loads are removed from Bus 20 and 39 as one option to maintain the normal operation. Fig. 11(c)–(d) prove that the frequency can recover to 60 Hz if the action is taken within 3 secs, while it will be below 60 Hz if the unload occurs 5 secs later; nevertheless, it is still within the operational range of the AC grid.

When the output power of all PV stations is decreasing at a rate of 0.2 MW/s due to sunset, the frequencies of synchronous generators drop. Shedding the load in the AC grid is effective in restoring the grid frequency within the ± 0.5 Hz perturbation range. Fig. 12(a) shows in Case 1, both Bus 20 and 39 remove 70 MW and 81.3 MW of load at 100 s and 306 s, respectively. However, if a three-phase fault occurs on Bus 21 at $t = 200$ s, the frequency will exceed the upper limit 60.5 Hz. Therefore, the loads to be shed are around 57 MW and 50 MW at 100 s and 226 s to contain the negative impact, which is given in Fig. 12(b) as Case 2. Fig. 12(c) gives the load condition on Bus 20 and 39,

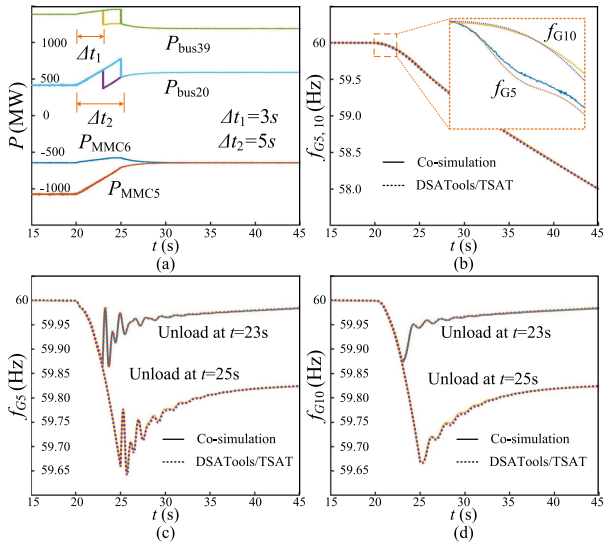


Fig. 11. The impact of solar irradiance on AC grid stability: (a) Power flow on Bus 20 and 39, and frequency response of generators 5 and 10 with Buses 20 and 39 (b) having no action, (c) unloading in 3 secs, and (d) unloading in 5 secs.

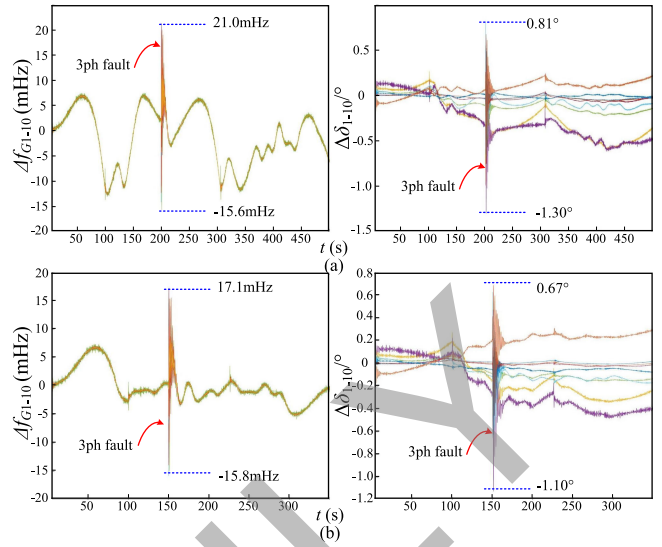


Fig. 13. Absolute generator frequency (left) and rotor angle (right) errors between proposed heterogeneous computing and TSAT simulation: (a) Case 1, and (b) Case 2.

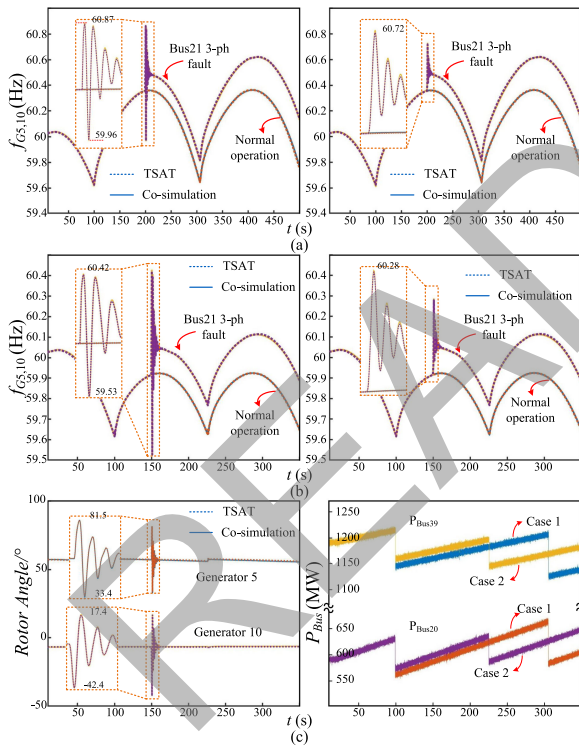


Fig. 12. AC grid dynamics under the impact of PV output power and 150 ms fault: (a)–(b) Generator 5 (left) and 10 (right) frequencies, and (c) generator rotor angles (left), Bus 20 and 39 load (right).

and the synchronous generators’ rotor angles of Case 2. The good agreement to DSATools/TSAT indicates the accuracy of the proposed co-simulation methodology.

In Fig. 13, the absolute frequency and rotor angle errors of all 10 synchronous generators are drawn to demonstrate the

TABLE II
AC/DC GRID SIMULATION SPEED COMPARISON

$N_{p1}:N_{p2}$	PV No.	CPU-GPU	CPU	MC-CPU	Sp1	Sp2
1:199	4.48×10^5	31.4s	238s	53.0s	7.6	1.7
10:190	8.8×10^5	67.3s	2340s	403s	35	6.0
50:150	2.8×10^6	274s	11575s	2360s	42	8.6
100:100	5.2×10^6	564s	22759s	4344s	40	7.7
150:50	7.6×10^6	1054s	31614s	10547s	30	10
199:1	9.952×10^6	1279s	39492s	14011s	31	11

accuracy of the proposed EMT-dynamic co-simulation using heterogeneous computing. It indicates that in both cases the maximum error appears when the three-phase fault occurs. Nevertheless, the maximum frequency errors are merely 21.0 mHz and 17.1 mHz for the two cases, respectively, whilst that of the rotor angle does not exceed -1.3° and -1.1° . Therefore, the insignificant errors thoroughly demonstrate the validity of the proposed modeling and computing method, meaning the heterogeneous parallel CPU-GPU co-simulation platform can also be used for power system study, operation, and planning with a much faster speed since it resembles DSATools in terms of results.

Table II summarizes the execution time that the platform requires to perform a 10 s simulation of the overall AC/DC grid where the CPU times are estimated based on a shorter duration. The inclusion of less parallel AC/DC grid slightly reduces the speedups over pure CPU cases compared with the previous table, since the PV modules account for the major computational burden. Similarly, the co-simulation is still faster than that of the 80-core CPU when the NVIDIA GTX 1080 GPU is utilized for solving the entire system, since tests show that even the last case, i.e., $N_{p1} : N_{p2} = 199$, can be completed within 2886 s while the corresponding data provided in Table II is around 40000 s and 14000 s for single- and multi-core CPU, respectively.

VI. CONCLUSION

This work introduces the EMT-dynamic co-simulation of the massive PV-integrated AC/DC grid using heterogeneous CPU-GPU computing. The proposed scalable PV model combining the discrete Norton equivalent circuits and their lumped counterpart is able to reflect the individuality of each PV panel in addition to maintaining a low computational burden. Meanwhile, the two processors are designed to be in charge of tasks that best suit them. The massively parallel architecture of the GPU featuring single-instruction multiple-thread is utilized to expedite the EMT process of millions of PV modules that otherwise will be a severe challenge to the CPU, which is more efficient in performing dynamic simulation of the remaining less repetitive AC grid. A maximum possible concurrency is attained following appropriate exploitation of a CUDA C kernel's capability to invoke a predefined number of threads with the same property to ensure the homogeneity of PV panels caters to the SIMT implementation mode. The tremendous time-step disparity between the two simulations enabled the adoption of multi-rate to avoid unnecessary computations. With a nearly 50 times speedup over CPU calculation using the same model, it is feasible to obtain the exact output power of PV plants by the GPU parallel processing whereas off-line EMT tools are unable to achieve. Therefore, the exact environmental impact on the PV stations and the power system transient stability can be studied efficiently in the proposed co-simulation, and the results are validated by commercial transient simulation tools. The proposed heterogeneous CPU-GPU computing approach provides an efficient solution for other electrical systems integrated with numerous elements.

APPENDIX

The 1STH-215-P PV module parameters: $S_{irr}^* = 1000 \text{ W/m}^2$, $\alpha_T = 0.1017\%/^\circ\text{C}$, $T_K^* = 273.15 \text{ K}$, $I_{0s} = 2.9259 \times 10^{-10} \text{ A}$, $V_{T0} = 1.5125 \text{ V}$, $I_{ph}^* = 7.8649 \text{ A}$, $R_s = 0.39383 \Omega$, $R_p = 313.3991 \Omega$.

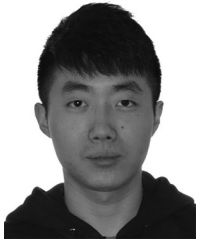
REFERENCES

- [1] E. Romero-Cadaval, B. Francois, M. Malinowski, and Q. Zhong, "Grid-connected photovoltaic plants: An alternative energy source, replacing conventional sources," *IEEE Ind. Electron. Mag.*, vol. 9, no. 1, pp. 18–32, Mar. 2015.
- [2] M. J. Carrizosa, A. Arzandé, F. D. Navas, G. Damm, and J. Vannier, "A control strategy for multiterminal DC grids with renewable production and storage devices," *IEEE Trans. Sustain. Energy*, vol. 9, no. 2, pp. 930–939, Apr. 2018.
- [3] D. Lew *et al.*, "The power of small: The effects of distributed energy resources on system reliability," *IEEE Power Energy Mag.*, vol. 15, no. 6, pp. 50–60, Nov. 2017.
- [4] G. Lammert, D. Premm, L. D. P. Ospina, J. C. Boemer, M. Braun, and T. Van Cutsem, "Control of photovoltaic systems for enhanced short-term voltage stability and recovery," *IEEE Trans. Energy Convers.*, vol. 34, no. 1, pp. 243–254, Mar. 2019.
- [5] P. H. Divshali and L. Söder, "Improving PV dynamic hosting capacity using adaptive controller for STATCOMs," *IEEE Trans. Energy Convers.*, vol. 34, no. 1, pp. 415–425, Mar. 2019.
- [6] A. Chakraborty and A. Bose, "Smart grid simulations and their supporting implementation methods," *Proc. IEEE*, vol. 105, no. 11, pp. 2220–2243, Nov. 2017.
- [7] W. Xiao, F. F. Edwin, G. Spagnuolo, and J. Jatskevich, "Efficient approaches for modeling and simulating photovoltaic power systems," *IEEE J. Photovolt.*, vol. 3, no. 1, pp. 500–508, Jan. 2013.
- [8] E. I. Batzelis, I. A. Routsolias, and S. A. Papatthanassiou, "An explicit PV string model based on the Lambert W function and simplified MPP expressions for operation under partial shading," *IEEE Trans. Sustain. Energy*, vol. 5, no. 1, pp. 301–312, Jan. 2014.
- [9] L. Wei, R. J. Kerkman, R. A. Lukaszewski, H. Lu, and Z. Yuan, "A calculation method of photovoltaic array's operating point for MPPT evaluation based on one-dimensional Newton–Raphson method," *IEEE Trans. Ind. Appl.*, vol. 51, no. 1, pp. 567–575, Jan. 2015.
- [10] G. N. Psarros, E. I. Batzelis, and S. A. Papatthanassiou, "Partial shading analysis of multistring PV arrays and derivation of simplified MPP expressions," *IEEE Trans. Sustain. Energy*, vol. 6, no. 2, pp. 499–508, Apr. 2015.
- [11] J. Xu, A. M. Gole, and C. Zhao, "The use of averaged-value model of modular multilevel converter in DC grid," *IEEE Trans. Power Del.*, vol. 30, no. 2, pp. 519–528, Apr. 2015.
- [12] K. Ding, X. Bian, H. Liu, and T. Peng, "A MATLAB-Simulink-based PV module model and its application under conditions of nonuniform irradiance," *IEEE Trans. Energy Convers.*, vol. 27, no. 4, pp. 864–872, Dec. 2012.
- [13] A. Chatterjee, A. Keyhani, and D. Kapoor, "Identification of photovoltaic source models," *IEEE Trans. Energy Convers.*, vol. 26, no. 3, pp. 883–889, Sep. 2011.
- [14] M. J. Z. Zadeh and S. H. Fathi, "A new approach for photovoltaic arrays modeling and maximum power point estimation in real operating conditions," *IEEE Trans. Ind. Electron.*, vol. 64, no. 12, pp. 9334–9343, Dec. 2017.
- [15] A. Hariri and M. O. Faruque, "A hybrid simulation tool for the study of PV integration impacts on distribution networks," *IEEE Trans. Sustain. Energy*, vol. 8, no. 2, pp. 648–657, Apr. 2017.
- [16] J. Hu, Z. Li, J. Zhu, and J. M. Guerrero, "Voltage stabilization: A critical step toward high photovoltaic penetration," *IEEE Ind. Electron. Mag.*, vol. 13, no. 2, pp. 17–30, Jun. 2019.
- [17] J. Ma, X. Pan, K. L. Man, X. Li, H. Wen, and T. On Ting, "Detection and assessment of partial shading scenarios on photovoltaic strings," *IEEE Trans. Ind. Appl.*, vol. 54, no. 6, pp. 6279–6289, Nov. 2018.
- [18] S. Hosseini, S. Taheri, M. Farzaneh, and H. Taheri, "Modeling of snow-covered photovoltaic modules," *IEEE Trans. Ind. Electron.*, vol. 65, no. 10, pp. 7975–7983, Oct. 2018.
- [19] A. Mudlapur, V. V. Ramana, R. V. Damodaran, V. Balasubramanian, and S. Mishra, "Effect of partial shading on PV fed induction motor water pumping systems," *IEEE Trans. Energy Convers.*, vol. 34, no. 1, pp. 530–539, Mar. 2019.
- [20] Y. Mahmoud and W. Xiao, "Evaluation of shunt model for simulating photovoltaic modules," *IEEE J. Photovolt.*, vol. 8, no. 6, pp. 1818–1823, Nov. 2018.
- [21] Z. Zhou and V. Dinavahi, "Parallel massive-thread electromagnetic transient simulation on GPU," *IEEE Trans. Power Del.*, vol. 29, no. 3, pp. 1045–1053, Jun. 2014.
- [22] Z. Zhou and V. Dinavahi, "Fine-grained network decomposition for massively parallel electromagnetic transient simulation of large power systems," *IEEE Power Energy Technol. Syst. J.*, vol. 4, no. 3, pp. 51–64, Sep. 2017.
- [23] N. Lin and V. Dinavahi, "Exact nonlinear micromodeling for fine-grained parallel EMT simulation of MTDC grid interaction with wind farm," *IEEE Trans. Ind. Electron.*, vol. 66, no. 8, pp. 6427–6436, Aug. 2019.
- [24] NVIDIA Corp, NVIDIA Tesla V100 GPU architecture, Aug. 2017.
- [25] E. Muljadi, M. Singh, and V. Gevorgian, "PSCAD modules representing PV generator," National Renewable Energy Lab. (NREL) Technical Reports, Aug. 2013.
- [26] H. Selhi, C. Christopoulos, A. F. Howe, and S. Y. R. Hui, "The application of transmission-line modelling to the simulation of an induction motor drive," *IEEE Trans. Energy Convers.*, vol. 11, no. 2, pp. 287–297, Jun. 1996.
- [27] NVIDIA Corp, CUDA C programming guide, May 2019.
- [28] M. Hagiwara and H. Akagi, "Control and experiment of pulsewidth-modulated modular multilevel converters," *IEEE Trans. Power Electron.*, vol. 24, no. 7, pp. 1737–1746, Jul. 2009.
- [29] S. Shongwe and M. Hanif, "Comparative analysis of different single-diode PV modeling methods," *IEEE J. Photovolt.*, vol. 5, no. 3, pp. 938–946, May 2015.



performance computing of integrated AC/DC grids.

Ning Lin (Member, IEEE) received the B.Sc. and M.Sc. degrees in electrical engineering from Zhejiang University, Hangzhou, China, in 2008 and 2011, respectively, and the Ph.D. degree in electrical and computer engineering from the University of Alberta, Edmonton, AB, Canada, in 2018. From 2011 to 2014, he was an Engineer on FACTS and HVdc. His research interests include electromagnetic transient simulation, real-time hardware-in-the-loop emulation of power systems and power electronic systems, massively parallel processing, and heterogeneous high-



Shiqi Cao (Student Member, IEEE) received the B.Eng. degree in electrical engineering and automation from the East China University of Science and Technology, Shanghai, China, in 2015, and the M.Eng. degree in power system from Western University, London, ON, Canada, in 2017. He is currently working toward the Ph.D. degree in electrical and computer engineering with the University of Alberta, Edmonton, AB, Canada. His research interests include power system dynamic simulation and stability analysis.



interests include real-time simulation of power systems and power electronic systems, electromagnetic transients, device-level modeling, large-scale systems, and parallel and distributed computing.

Venkata Dinavahi (Fellow, IEEE) received the B.Eng. degree in electrical engineering from the Visveswaraya National Institute of Technology (VNIT), Nagpur, India, in 1993, the M.Tech. degree in electrical engineering from the Indian Institute of Technology (IIT) Kanpur, India, in 1996, and the Ph.D. degree in electrical and computer engineering from the University of Toronto, Ontario, Canada, in 2000. He is currently a Professor with the Department of Electrical and Computer Engineering, University of Alberta, Edmonton, AB, Canada. His research

READ ONLY